Supporting Information

Multi-Functional interface modulation through thiol functionalized covalent organic frameworks for efficient and durable perovskite solar cells

Bo Yu, Kai Wang, Yapeng Sun, Huangzhong Yu*

School of Physics and Optoelectronics, South China University of Technology, Guangzhou 510640, Guangdong, China.

* Corresponding author: hzhyu@scut.edu.cn (Huangzhong Yu).

Experimental section

Materials

The indium tin oxide (ITO, 15 Ω sq^{-1}) was provided via Wuhu Jinghui Electronic Technology Co., Ltd); Chlorobenzene (CB, 99.9%), N, N-dimethylformamide (DMF, 99.8%), and isopropanol (IPA, 99.5%) were from Sigma-Aldrich; Dimethyl sulfoxide (DMSO, 99.9%) was from Alfa Aesar; Perovskite precursor reagents, Phenyl-C61-butyric acid methyl ester (PCBM, 99%) and [2-(3,6-Dimethoxy-9H-carbazol-9-yl)ethyl]phosphonic Acid (MeO-2PACz, 99%) were purchased Xi'an Polymer Light Technology Corp., China; Bathocuproine (BCP, >98%), 2,5-diaminobenzene-1,4-dithiol dihydrochloride (99.9%) and 1,3,5-triformylphloroglucinol (99.9%) were obtained from Aladdin Reagent Co., Ltd; All the commercial materials were from commercial channels and used without further treatment.

Preparation of thiol-functionalized COFs

Thiol-functionalized COFs (SH-COF) were synthesized by two kinds of precursors based on the Schiff-base reactions. 1,3,5-triformylphloroglucinol (TFP) (63 mg, 0.3 mmol) and 2,5-diaminobenzene-1,4-dithiol dihydrochloride (DBD) (110 mg, 0.45 mmol) were precisely weighted and added to a 10 mL Schlenk glass reaction tube. Then, 1.5 mL of mesitylene, 1.5 mL of dioxane and 0.5 mL of 3 M acetic acid was transferred into the container. The mixture was ultrasonicated for 30 min in order to uniformly dispersed. After three freeze-thaw degassing treatments in liquid N_2 bath, the tube was heated at 120 °C for 72 h. After cooling to room temperature, the separated precipitate was washed for 5 times with tetrahydrofuran, and dried in vacuum at 180 °C for 24 h to obtain the dark red product. Subsequently, SH-COF powder was dispersed in IPA solution and stirred overnight to obtain relevant suspension for subsequent experiments.

Device fabrication

The pre-patterned indium tin oxide (ITO) substrates were sequentially ultrasonically washed with detergent, deionized water, acetone and isopropanol for 15 min. The processed substrates were further cleaned with O_3/ultraviolet treatments for

15 min and finally transferred to a N_2-filled glovebox before used. For the hole-transporting layer, MeO-2PACz solution (0.5 mg ml^{-1} in ethyl alcohol) was spin-coated on the ITO substrate at 3000 rpm for 30 s, and then annealed at 100 °C for 10 min. The Perovskite precursor solution ($FA_{0.95}Cs_{0.05}PbI_3$) was obtained by mixing FAI, PbI_2, and CsI in DMF: DMSO mixed solvent (volume ratio: 4 to 1). The perovskite films were deposited on the above substrates by a two-step spin-coating process, 2000 rpm for 10 s and 4000 rpm for 30s, respectively. 150 μL CB as anti-solvent was poured on the spinning film at 35 s and then annealed at 100 °C for 30 min. Then, $PC_{61}BM$ (20 mg mL^{-1} in CB) and BCP (0.5 mg mL^{-1} in IPA) solutions were spin-coated onto the substrates at 3000 rpm for 40 s and 6000 rpm for 30 s, respectively. Next, 30 μL of SH-COF suspension (0, 1, 2, 3 and 5 mg mL^{-1} in IPA) was deposited on the above films at 4000 rpm for 30 s. Finally, a 90 nm Ag electrode was obtained by means of thermal evaporation under high-vacuum (less than 2.8×10^{-4} Pa).

Characterization

The X-ray diffraction (XRD) curves were measured on a Bruker Discovery D8 diffractometer with Cu-Kα radiation (λ=1.54 Å) at 40 kV. Fourier transform infrared (FTIR) spectra were characterized on a Thermo Scientific Nicolet iS50 instrument. X-ray photoelectron spectroscopy (XPS) and ultraviolet photoelectron spectroscopy (UPS) were carried out on the Thermo Scientific Escalab 250Xi instrument equipped with Mg-Kα source. The morphological properties of the perovskite films were identified via a field emission scanning electron microscopy (SEM, Hitachi S4700). The atomic force microscope (AFM) was investigated on the Multimode 8 AFM from Bruker. UV-Vis absorption spectra of the perovskite films were obtained on an ocean optics spectrum testing system with DH-2000-BAL UV-VIS-NIR light source. Steady-state photoluminescence (PL) spectra were measured by performing a Laser405-1HS illuminant. Time-resolved PL (TRPL) measurements were performed using a FLS920 from Edinburgh Instruments Ltd./UK. The current density-voltage (*J-V*) measurements and space-charge-limited current (SCLC) performance were executed through a Keithley 2400 source meter equipped with a xenon lamp-based solar simulator (AM 1.5G, irradiance of 100 $mW \cdot cm^{-2}$). The external quantum efficiency (EQE) was

recorded with AC mode on an SRF50 system. The electrochemical impedance spectra (EIS) were measured using a Zennium-IM6 electrochemical workstation under dark conditions.

Theoretical calculation details

We have used the first-principles Vienna Ab Initio Package (VASP) to complete all calculations. The exchange correlation functional is described by the Perdue-Burke-Ernzerhof (PBE) method in the generalized gradient approximation (GGA) with the plane wave cut-off energy of 450 eV. For the optimization process, the electron energy is self-consistent when it is converged to the accuracy of 1×10^{-5} eV, and the convergence criteria for atomic forces are set at less than 0.03 eV/Å. The Brillouin zone is divided by the number of K-point grids centered on the Γ point. While 1×2×1 grid of K-points is used for electronic states analysis. The DFT-D3 method of Grimme is enabled to describe the dispersion interactions. The differential charge density between SH-COF molecules and Ag is defined as Δ ρ, $\Delta\rho = \rho_{AB} - \rho_A - \rho_B$, where ρ_{AB} represents the structure charge density after interface optimization, ρ_A represented the charge density of SH-COF, ρ_A represented the charge density of Ag. The adsorption energy (E_{ads}) of SH-COF molecules on the Ag surface is defined as E_{ads}, $E_{ads} = E_{A+B} - E_A - E_B$, where E_{A+B}, E_A, E_B were the total energy of SH-COF molecules are adsorbed on the Ag surface, the energy of SH-COF molecules, the energy of the Ag film, respectively.

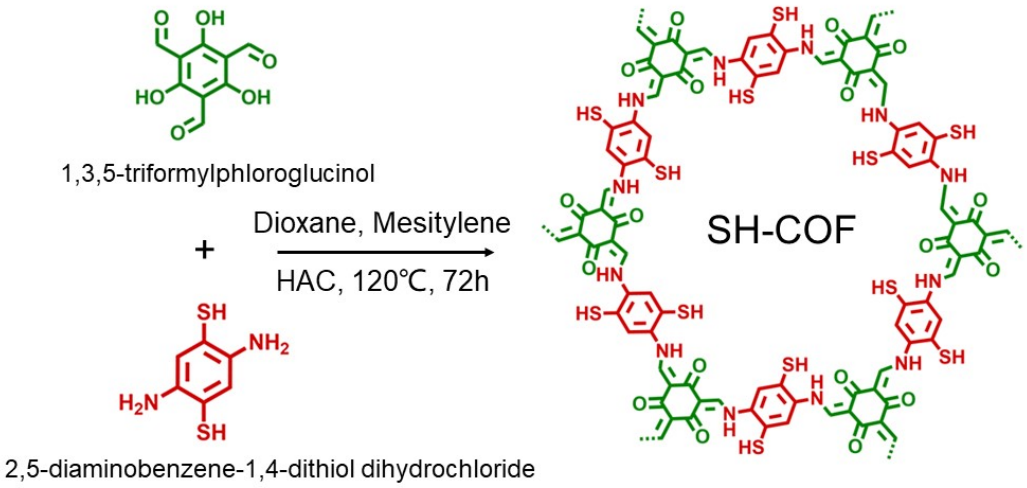

Figure S1. The synthesis scheme of SH-COF.

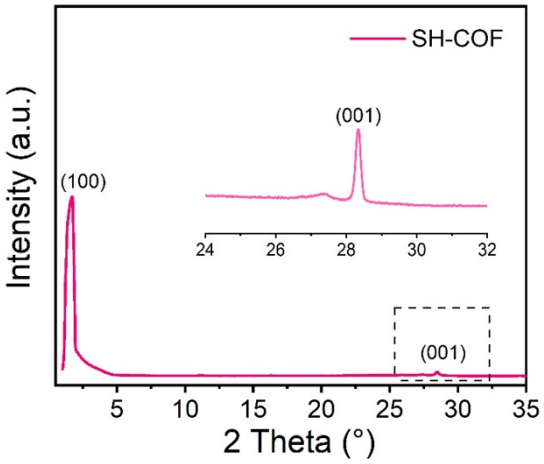

Figure S2. The XRD pattern of SH-COF.

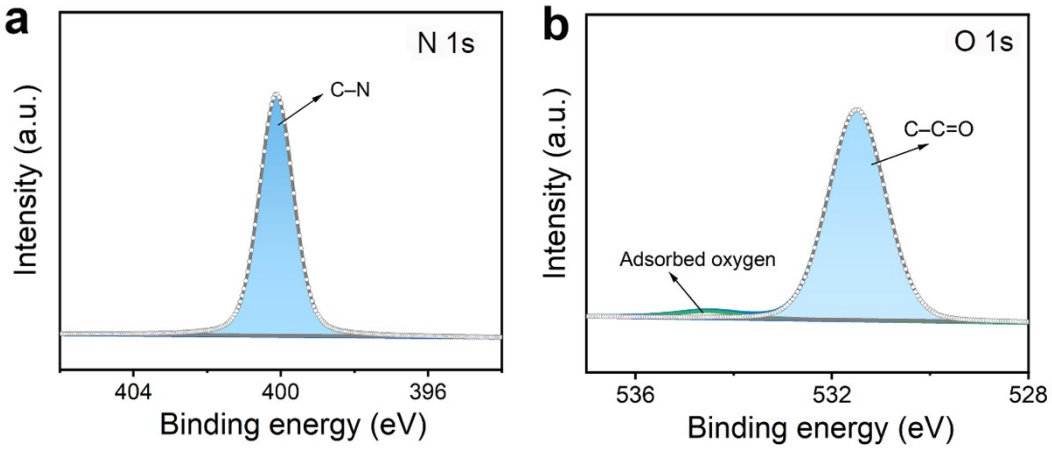

Figure S3. XPS pattern of **a**) N 1s and **b**) O 1s peaks of SH-COF.

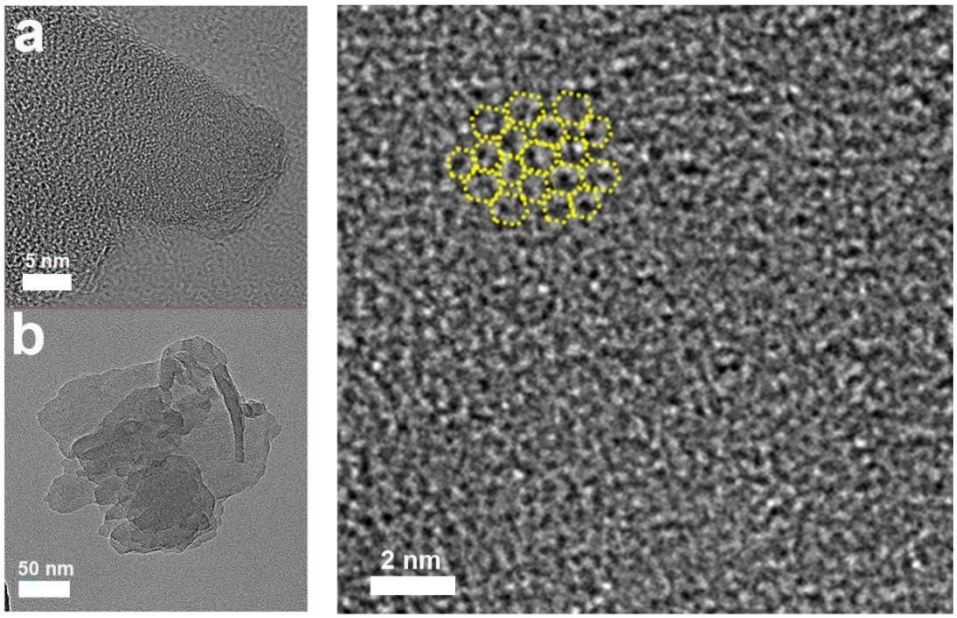

Figure S4. High-resolution transmission electron microscopy (TEM) image of SH-COF.

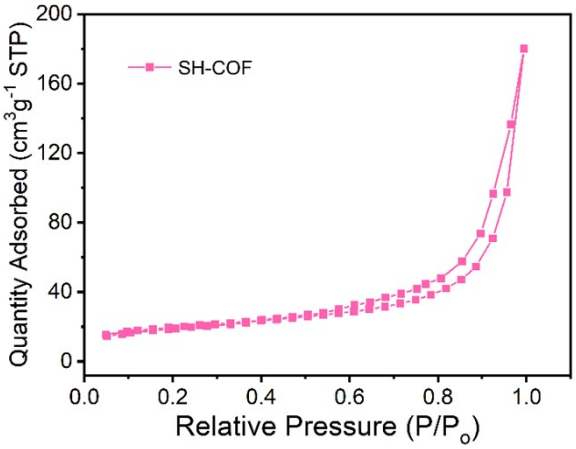

Figure S5. N_2 adsorption/desorption isotherms of SH-COF.

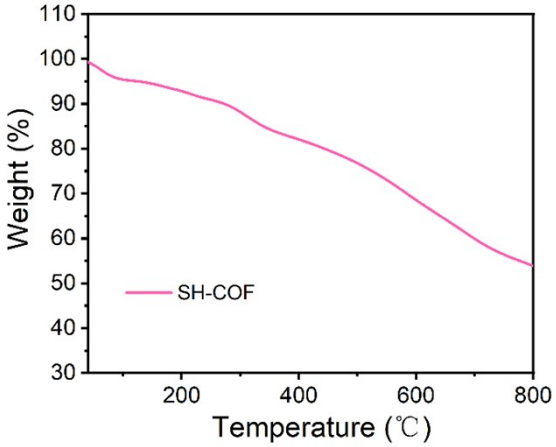

Figure S6. The weight and temperature dependence of SH-COF.

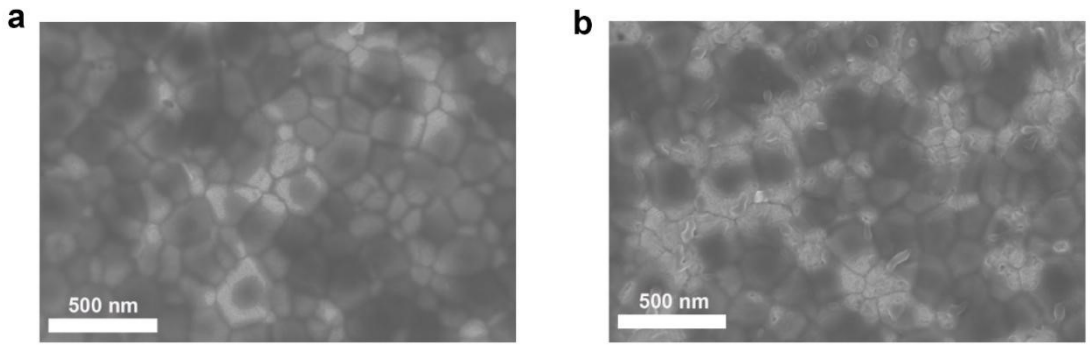

Figure S7. Top-view SEM images of **a**) perovskite/PCBM and **b**) perovskite/PCBM/SH-COF films.

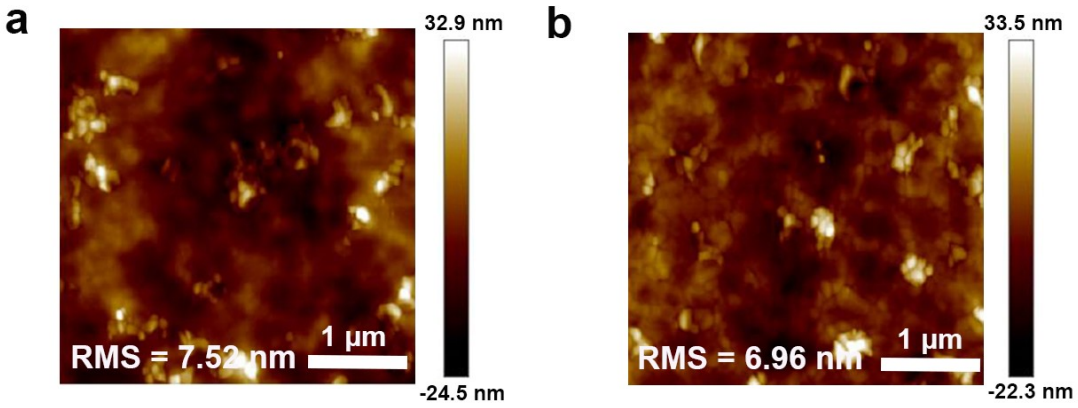

Figure S8. AFM images of **a**) perovskite/PCBM and **b**) perovskite/PCBM/SH-COF films.

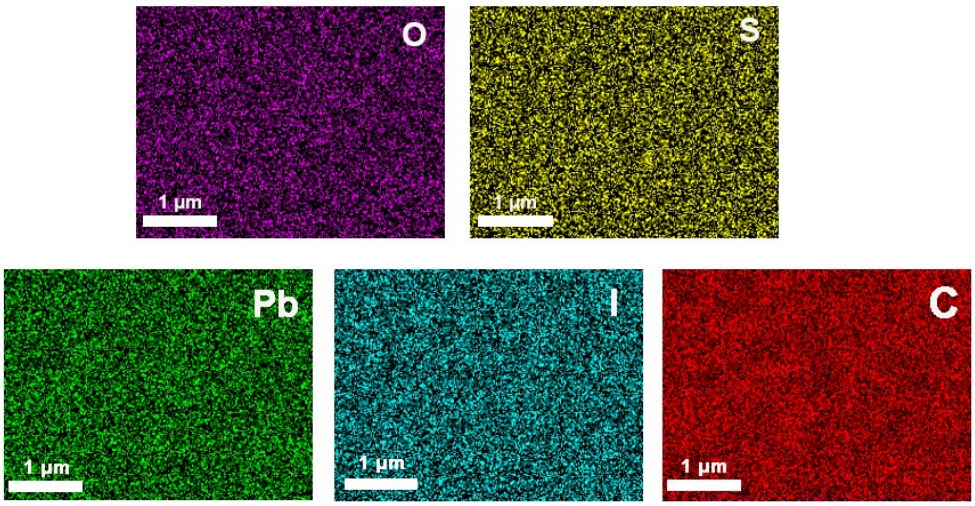

Figure S9. EDS mapping of C, Pb, I, S, O elements of the perovskite/PCBM/SH-COF film.

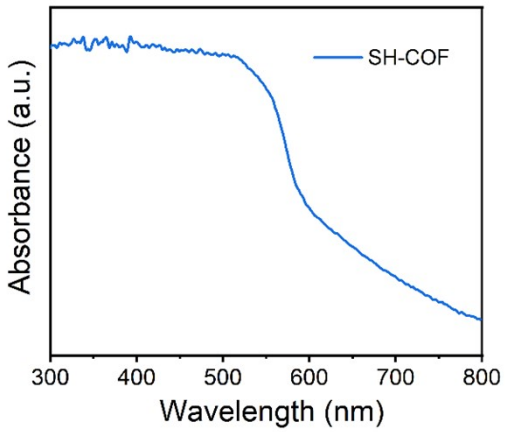

Figure S10. UV-vis diffuse reflectance spectrum of SH-COF.

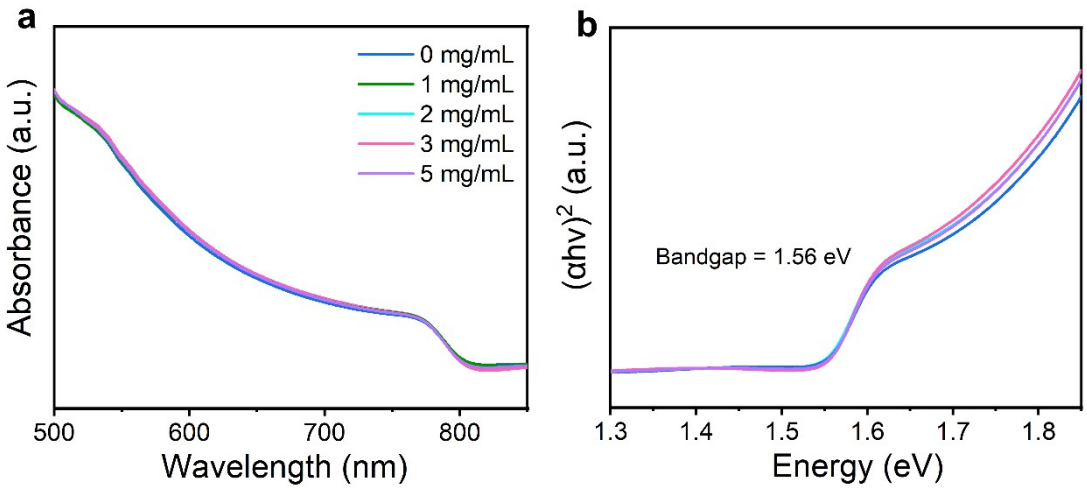

Figure S11. a) UV-vis spectra of perovskite/PCBM/SH-COF films with different concentrations of SH-COF, and **b**) the Tauc plot of the perovskite film.

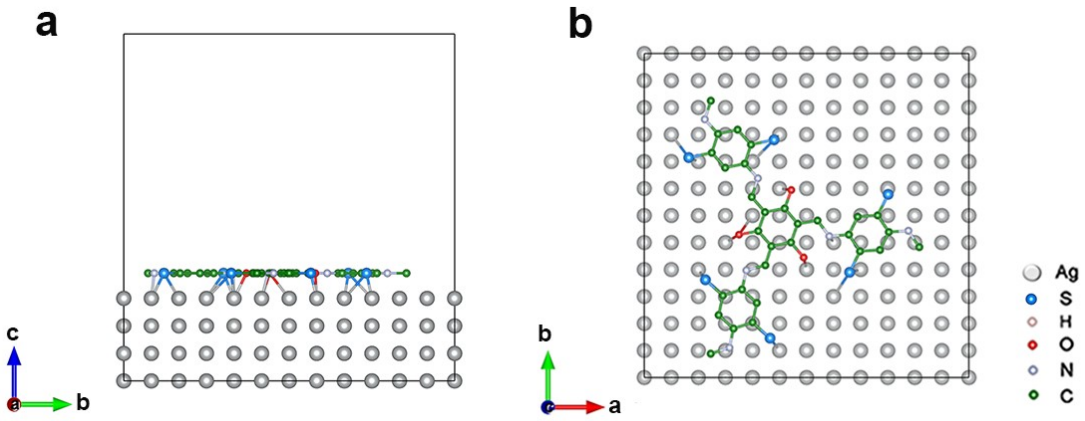

Figure S12. The theoretical model of SH-COF molecule and Ag before optimization: **a**) front view and **b**) top view.

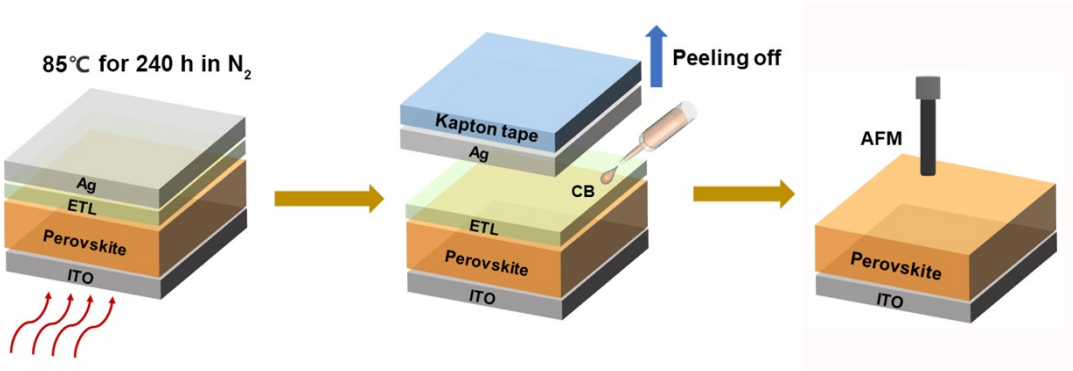

Figure S13. The preparation process of perovskite films from the aging devices for AFM characterizations, the corresponding device structure is ITO/perovskite/PCBM/BCP/SH-COF/Ag.

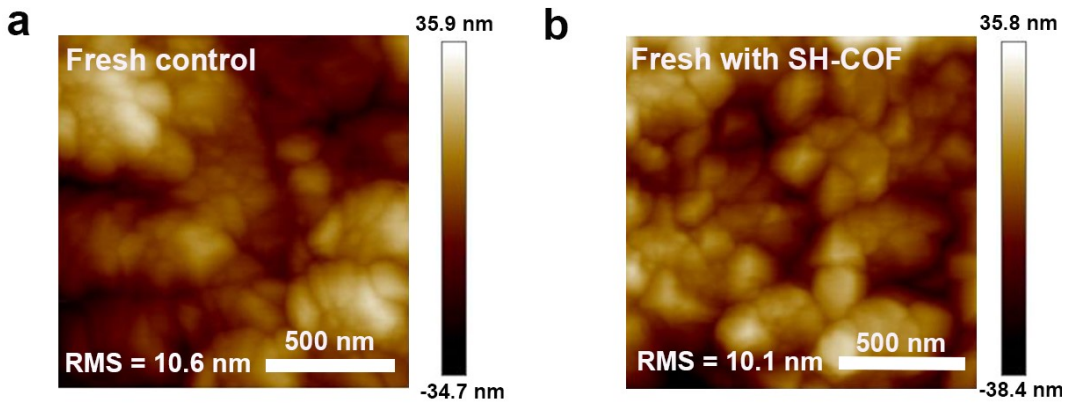

Figure S14. AFM images of perovskite films from the devices **d**) without and **e**) with SH-COF before thermal aging.

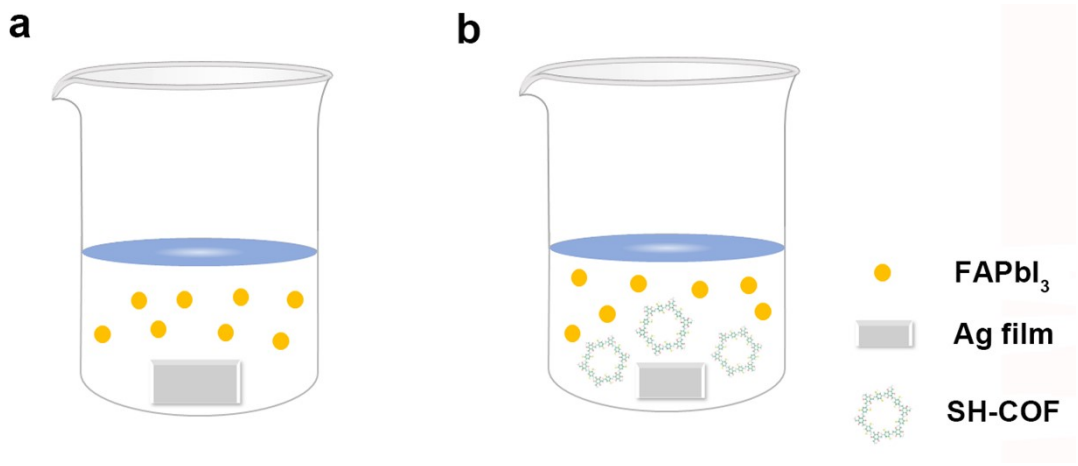

Figure S15. Schematic diagram of immersing experiments. The Ag/ITO films are immersed in $FAPbI_3$ dispersion (15 mg mL^{-1} in isopropanol) without or with SH-COF (5.0 mg mL^{-1}).

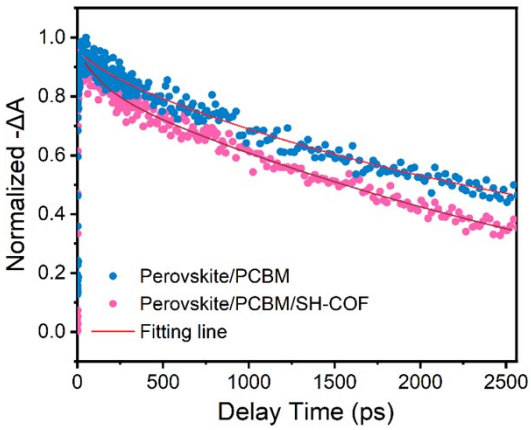

Figure S16. TA spectra as a function of delay time for perovskite/PCBM and perovskite/PCBM/SH-COF films.

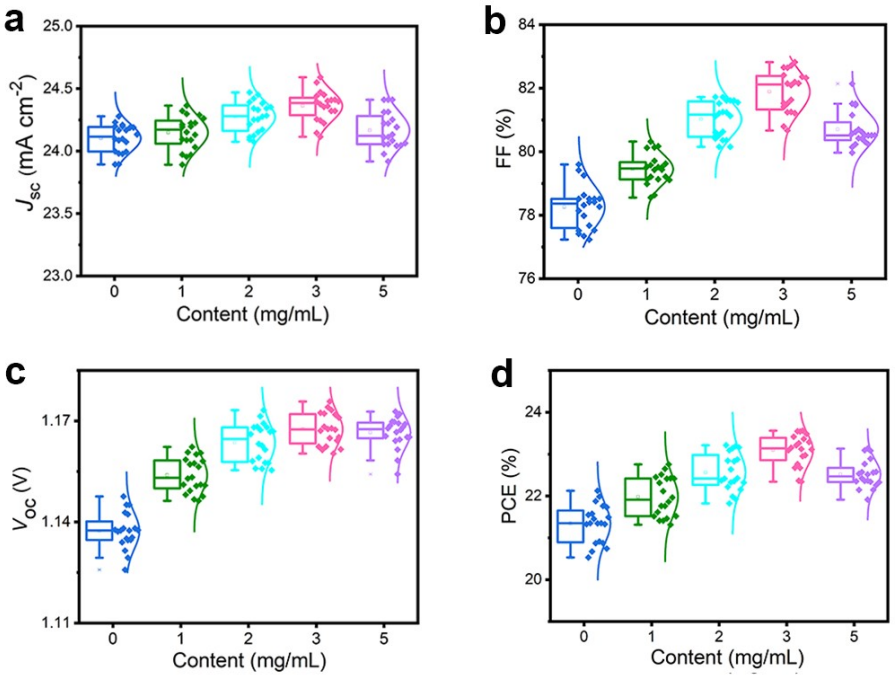

Figure S17. Statistical distribution of the devices with different concentrations of SH-COF of **a**) J_{SC}, **b**) FF, **c**) V_{OC}, and **d**) PCE.

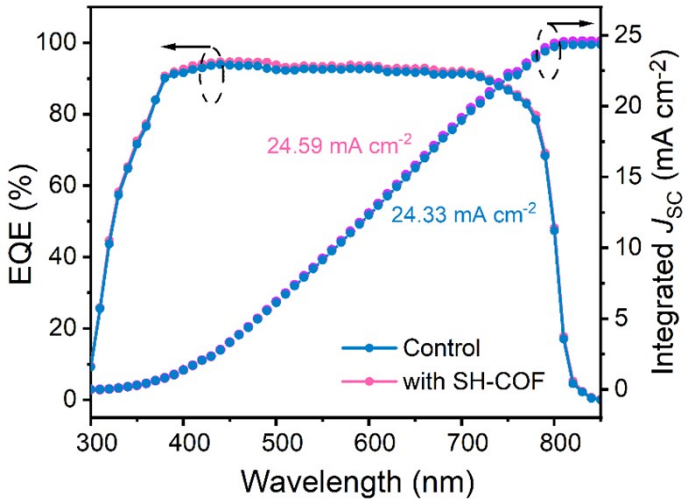

Figure S18. EQE curves of the control and SH-COF modified devices.

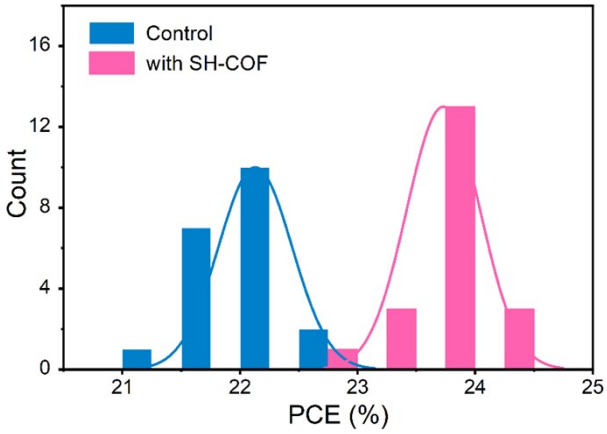

Figure S19. Statistics of PCE distribution of the devices with and without SH-COF layer (20 devices).

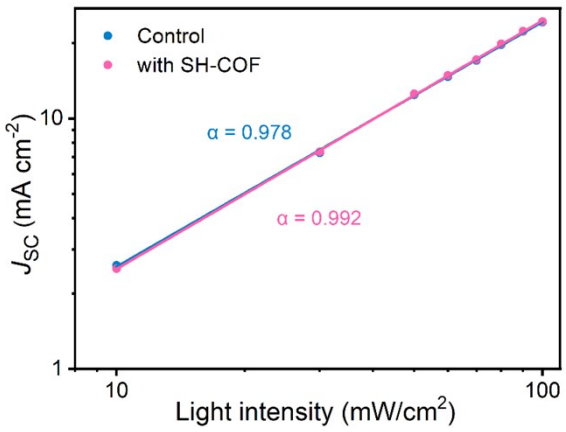

Figure S20. J_{sc} versus light intensity plots of the control and SH-COF modified devices.

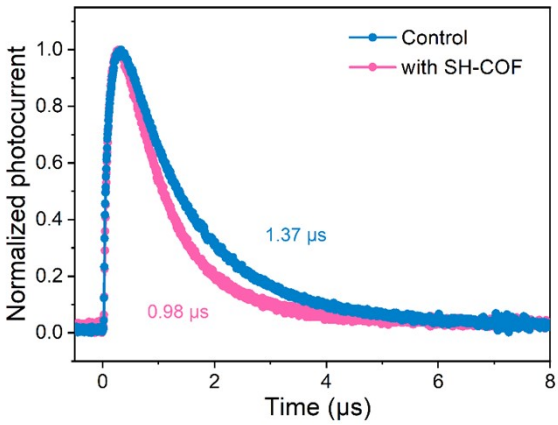

Figure S21. TPC curves of the control and SH-COF modified devices.

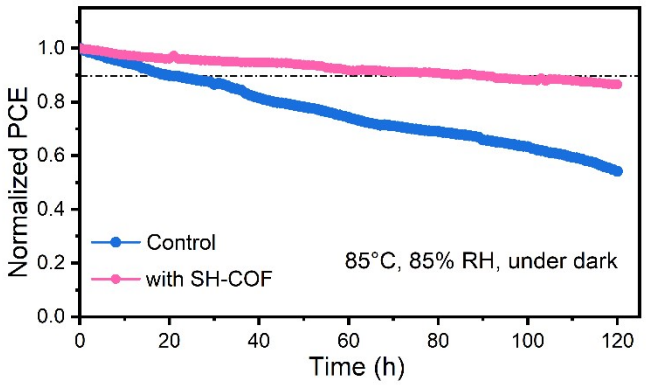

Figure S22. The long-term operational stability of the unencapsulated devices during 85℃ and 85% RH aging.

Table S1. Summary of fitting parameters of time-resolved PL (TRPL) spectra.

Sample	A_1	τ_1 (ns)	A_2	τ_2 (ns)	τ_{ave} (ns)
Perovskite	4634.5	68.94	5235	5.59	63.59
Perovskite/SH-COF	2116.1	26.73	7982	3.74	18.79
Perovskite/PCBM	2850.7	19.01	6931	3.51	14.21
Perovskite/PCBM/SH-COF	942.1	18.03	7970	2.32	9.84

The average carrier lifetime (τ_{ave}) is obtained by the following formula: $\tau_{ave} = (A_1\tau_1+A_2\tau_2)/(A_1+A_2)$, where A_1 and A_2 are the fitting amplitudes.

Table S2. The average *J-V* performance of the devices with different concentrations of SH-COF.

(The values are obtained from 20 devices)

SH-COF (mg mL^{-1})	***J*sc** (mA cm^{-2})	***V*oc** (V)	**FF** (%)	**PCE** (%)
0	24.10±0.11	1.14±0.005	78.25±0.66	21.34±0.43
1	24.15±0.13	1.15±0.005	79.45±0.47	21.98±0.46
2	24.27±0.12	1.16±0.006	81.03±0.55	22.56±0.44
3	24.36±0.12	1.17±0.004	81.89±0.64	23.10±0.36
5	24.17±0.14	1.16±0.004	80.71±0.54	22.52±0.32

Table S3. Solar cell performance parameters of the champion devices with and without SH-COF.

Sample	J_{sc} **(mA cm^{-2})**	V_{oc} **(V)**	**FF (%)**	**PCE (%)**
Control	24.61	1.134	79.73	22.25
Control	24.79	1.142	80.15	22.69
with SH-COF	24.98	1.172	82.14	24.05
with SH-COF	25.02	1.173	82.18	24.12

Table S4. Comparison of PCE and thermal stability of PSCs with different barrier materials.

Device structure	Barrier	PCE	Thermal stability test	% of PCE is maintained	Year
FTO/PEDOT:PSS/$MAPbI_3$/PCBM/AZO/SnO_x/Ag	AZO/SnO_x	12.8%	Dark, 60°C in N_2, 1032 h	100%	2017[1]
FTO/NiMgLiO/$MAPbI_3$/PCBM/CeO_x/Ag	CeO_x	18.69%	MPP condition in air, 200 h	91%	2018[2]
FTO/NiMgLiO/$FAMACsPbI_3$/PCBM/BCP/Bi/Ag	Bi	18.67%	Dark, 85°C in N_2, 500 h	85.2%	2019[3]
ITO/NiO_x/$FA_{0.85}MA_{0.15}Pb(I_{0.75}Br_{0.25})_3$/PCBM-$C_3N_4$/BCP/Ag	C_3N_4	15.6% (36 cm^2)	Dark, 85°C in N_2, 1000 h	95%	2019[4]
ITO/P3CT/$MAPbI_3$/PCBM/C_{60}/TPBi/BTA/Cu	BTA	19.56%	Dark, 85 °C in N_2, 1100 h	90.7%	2020[5]
ITO/PTAA/CsFAMAPbI_3/PCBM/CIL/Au	CIL	20%	MPP condition in N_2, 250 h	80%	2021[6]
ITO/NiO_x/CsFAMAPbI_3/PCBM/BCP:TTTS/Ag	TTTS	22.59%	Dark, 85°C in N_2, 1500 h	93%	2022[7]
ITO/PTAA/$MAPbI_3$/PCBM/OXD-7/Ag	OXD-7	21.83%	Dark, 85°C in N_2, 1080 h	80%	2023[8]
ITO/PTAA/$FA_{0.95}Cs_{0.05}PbI_3$/C_{60}/ALD-SnO_2/amp-ZrN_x/Cu	amp-ZrN_x	23.1%	Dark, 85°C in N_2, 1100 h	90%	2023[9]
FTO/MeO-2PACz/RbCsMAFA$Pb(I_{0.95}Br_{0.05})_3$/PCBM/YbO_x/Cu	YbO_x	25.2%	Dark, 85°C in N_2, 500 h	98%	2024[10]
ITO/MeO-2PACz/$FA_{0.95}Cs_{0.05}PbI_3$/PCBM/BCP/SH-COF/Ag	SH-COF	24.12%	Dark, 85°C in N_2, 1200 h	93.3%	This work

Table S5. Solar cell performance parameters of the champion devices with and without SH-COF for the area of 1.0 cm^2.

Sample	***J*sc (mA cm^{-2})**	***V*oc (V)**	**FF (%)**	**PCE (%)**
Control	23.83	1.11	75.95	20.09
with SH-COF	24.12	1.15	77.98	21.63

Table S6. EIS fitting parameters of the control and SH-COF modified devices.

Sample	R_S (Ohm)	R_{rec} (Ohm)	C_{rec} (F)
Control	147.6	12368	3.45×10^{-8}
with SH-COF	137.1	25958	2.43×10^{-8}

References

1. K.O. Brinkmann, J. Zhao, N. Pourdavoud, T. Becker, T. Hu, S. Olthof, K. Meerholz, L. Hoffmann, T. Gahlmann, R. Heiderhoff, M. F. Oszajca, N. A. Luechinger, D. Rogalla, Y. Chen, B. Cheng, T Riedl, *Nat. Commun.* 2017, **8**, 13938.

2. R. Fang, S. Wu, W. Chen, Z. Liu, S. Zhang, R. Chen, Y. Yue, L. Deng, Y. Cheng, L. Han, W. Chen, *ACS Nano*, 2018, **12**, 2403–2414.

3. S. Wu, R. Chen, S. Zhang, B. Babu, Y. Yue, H. Zhu, Z. Yang, C. Chen, W. Chen, Y. Huang, S. Fang, T. Liu, L. Han, W. Chen, *Nat. Commun.* 2019, **1**, 1161.

4. E. Bi, W. Tang, H. Chen, Y. Wang, J. Barbaud, T. Wu, W. Kong, P. Tu, H. Zhu, X. Zeng, J. He, S. Kan, X. Yang, M. Grätzel, L. Han, *Joule* 2019, **3**, 2748–2760.

5. X. Li, S. Fu, W. Zhang, S. Ke, W. Song, J. Fang, *Sci. Adv.* 2020, **51**, eabd1580

6. J. Wang, J. Li, Y. Zhou, C. Yu, Y. Hua, Y. Yu, R. Li, X. Lin, R. Chen, H. Wu, H. Xia, H.-L. Wang, *J. Am. Chem. Soc.* 2021, **20**, 7759-7768.

7. J. Yang, Q. Cao, T. Wang, B. Yang, X. Pu, Y. Zhang, H. Chen, I. Tojiboyev, Y. Li, L. Etgar, X. Li, A. Hagfeldt, *Energy Environ. Sci.* 2022, **5**, 2154-2163.

8. N. Liu, J. Xiong, Z. He, C. Yuan, J. Dai, Y. Zhang, C. Zhou, X. Zhang, L. Li, D. Wang, Z. Zhang, Y. Huang, Q. Dai, J. Zhang *Adv. Energy Mater.* 2023, **13**, 2300025.

9. M. Xiao, G. Yuan, Z. Lu, J. Xia, D. Li, Y. Chen, Y. Zhang, F. Pei, C. Chen, Y. Bai, T. Song, J. Dou, Y. Li, Y. Chen, Z. Xu, X. Yang, Z. Liu, X. Liu, C. Zhu, Q. Chen *Adv. Mater.* 2023, **35**, 2301684.

10. Q. Li, L. Zhao, C. Hou, Y. You, J. Shyue, D. Wang, X. Li, Q. Zhao, Q. Gong, Z. Lu, Henry J. Snait, H. Yan, T. Huang, M. Yu, Q. Li, L. Zhao, C. Hou, Y. You, J. Shyue, D. Wang, X. Li, Q. Zhao, Q. Gong, Z. Lu, H.J. Snaith, R. Zhu, *Nature* 2024, **625**, 516–522.